A cGAS-dependent response links DNA damage and senescence in alveolar epithelial cells

Schuliga, Michael; Kanwal, Amama; Read, Jane; Blokland, Kaj Erik Cornelis; Burgess, Janette K; Prêle, Cecilia M; Mutsaers, Steven E; Grainge, Christopher; Thomson, Claire; James, Allen

Published in:
American Journal of Physiology - Lung Cellular and Molecular Physiology

DOI:
10.1152/ajplung.00574.2020

A cGAS-dependent response links DNA damage and senescence in alveolar epithelial cells: A potential drug target in IPF

Michael Schuliga[1,2], Amama Kanwal[1,2], Jane Read[1,2], Kaj EC Blokland[1,2,3], Janette K Burgess[3], Cecilia M Prêle[4,5], Steven E Mutsaers[4,5], Christopher Grainge[2,6,7], Claire Thomson[1,2,8], Allen James[7], Nathan Bartlett[1,2], and Darryl A Knight[1,2,9]

[1]School of Biomedical Sciences and Pharmacy, University of Newcastle, Callaghan, NSW, Australia; [2]Priority Centre for Healthy Lungs, Hunter Medical Research Institute, New Lambton Heights, NSW, Australia; [3]University of Groningen, University Medical Center Groningen, Department of Pathology and Medical Biology, Groningen Research Institute of Asthma and COPD and KOLFF Institute, Netherlands; [4]Institute for Respiratory Health, University of Western Australia, Nedlands, WA, Australia; [5]Centre for Cell Therapy and Regenerative Medicine, School of Biomedical Sciences, University of Western Australia, Crawley, WA, Australia; [6]School of Medicine and Public Health, University of Newcastle, Callaghan, NSW, Australia; [7]John Hunter Hospital, Newcastle, NSW; [8]St Vincent's Hospital, Sydney, NSW; [9]Providence Health Care Research Institute, Vancouver, British Columbia, Canada.

Running title: The role of cGAS in alveolar epithelial cell senescence

Correspondence Dr. Michael Schuliga, School of Biomedical Sciences and Pharmacy, University of Newcastle, HMRI Building, Callaghan, NSW 2308, Australia, email: Michael.Schuliga@newcastle.edu.au

Data supplement: 10.6084/m9.figshare.13262993

ABSTRACT

Alveolar epithelial cell (AEC) senescence is implicated in the pathogenesis of idiopathic pulmonary fibrosis (IPF). Mitochondrial dysfunction including release of mitochondrial DNA (mtDNA) is a feature of senescence, which led us to investigate the role of the DNA-sensing GMP-AMP synthase (cGAS) in IPF, with a focus on AEC senescence. cGAS expression in fibrotic tissue from lungs of IPF patients was detected within cells immunoreactive for epithelial cell adhesion molecule (EpCAM) and p21, epithelial and senescence markers respectively. Submerged primary cultures of AECs isolated from lung tissue of IPF patients (IPF-AECs, n=5) exhibited higher baseline senescence than AECs from control donors (Ctrl-AECs, n=5-7), as assessed by increased nuclear histone 2AXγ phosphorylation, p21 mRNA and expression of senescence-associated secretory phenotype (SASP) cytokines. Pharmacological cGAS inhibition using RU.521 diminished IPF-AEC senescence in culture and attenuated induction of Ctrl-AEC senescence following etoposide-induced DNA damage. Short interfering RNA (siRNA) knockdown of cGAS also attenuated etoposide-induced senescence of the AEC line, A549. Higher levels of mtDNA were detected in the cytosol and culture supernatants of primary IPF- and etoposide-treated Ctrl-AECs when compared to Ctrl-AECs at baseline. Furthermore, ectopic mtDNA augmented cGAS-dependent senescence of Ctrl-AECs, whereas DNAse I treatment diminished IPF-AEC senescence. This study provides evidence that a self-DNA driven, cGAS-dependent response augments AEC senescence, identifying cGAS as a potential therapeutic target for IPF.

Key words: Alveolar epithelium, Idiopathic pulmonary fibrosis (IPF), cGAS, Mitochondrial DNA (mtDNA) and Senescence

INTRODUCTION

Idiopathic pulmonary fibrosis (IPF) is a progressive, fatal lung disease of unknown aetiology, with few treatment options (6, 7, 27). Age is a risk factor and appears to be a major driver of the disease; albeit through mechanisms that are not entirely understood (22). Cellular senescence, a hallmark of ageing is characterized by irreversible cell cycle arrest, increased resistance to apoptosis and the senescence-associated secretory phenotype (SASP) (37). Senescence is an outcome of genomic DNA damage caused primarily by telomere shortening and/or oxidative stress (ie as a consequence of mitochondrial dysfunction). There is accumulating evidence that senescence contributes to IPF, including the linkage of mutations that accelerate telomere attrition and the detection of senescent epithelial cells and fibroblasts in lung from IPF patients (2, 14, 19).

The enzyme GMP-AMP synthase (cGAS) detects double stranded DNA (dsDNA) in the cytoplasm to generate the cyclic dinucleotide cGAMP, a secondary messenger that elicits pro-inflammatory and type I interferon (IFN) responses. Apart from sensing bacterial and viral DNA in innate immunity, cGAS also binds and is activated by damaged endogenous DNA released from the nucleus and mitochondria (39, 42). Notably, a number of recent studies provide compelling evidence that cGAS activation by self-DNA is a driver of inflammatory lung disease ie asthma, COPD and silicosis (reviewed by Ma *et al* (20)). cGAS is also a crucial mediator of damaged DNA-induced cellular senescence (11, 42). The contribution of cGAS in senescence involves activation of the stimulator of interferon genes (STING) pathway and subsequent induction of the SASP, which perpetuates senescence via autocrine and paracrine processes. Our group recently provided evidence that damaged mitochondrial DNA (mtDNA) via the activation of cGAS augments lung fibroblast senescence; a process which may contribute to the pathogenesis of fibrotic lung diseases such

as IPF (32). To our knowledge, the role of cGAS in alveolar epithelial cell (AEC) senescence in the context of IPF pathology has not been previously evaluated (20).

MtDNA encodes essential protein subunits of the electron transport chain (ETC) which drive mitochondrial respiration. In close proximity to the ETC where reactive oxygen species (ROS) are formed, damage and subsequent mutations accumulate in mtDNA with age; resulting in mitochondrial dysfunction and collapse in mitochondrial membrane potential (15, 16). DNA released by dysmorphic mitochondria is a potent damage-associated molecular pattern (DAMP) that triggers inflammatory responses by binding pattern recognition receptors (PRRs), including cGAS and toll-like receptor 9 (TLR9) (40). The increased propensity for senescence of AECs and lung fibroblasts from IPF patients is associated with alterations in mitochondrial homeostasis and function (6, 7, 31). Ryu and colleagues recently showed that lung fibroblasts from IPF patients release increased amounts of mtDNA when compared to age-matched controls and that higher levels of cell free mtDNA in the bronchoalveolar lavage fluid (BALF) or serum of IPF patients predicts mortality (29). In another study, increased levels of oxidized and damaged mtDNA were detected in lung tissue of IPF patients as well as the supernatants of type 2 AECs (AEC2s) *in vitro* when subjected to endoplasmic reticulum (ER) and oxidative stress (7). These studies and others suggest that cell-derived, damaged mtDNA could play a key role in IPF pathology.

In this study, we investigated whether increased release of self (mt)DNA perpetuates AEC senescence via cGAS. To address this, we used AECs isolated from IPF patients (IPF-LFs) with high baseline senescence, or in cells from controls (Ctrl-AECs) that were induced to become senescent using etoposide. The levels of cytosolic and extracellular mtDNA formed by these cells were examined, as well as the effects of ectopic mtDNA and DNaseI on

100 senescence. Pharmacological intervention was used to determine the contribution of cGAS to
101 DNA-driven AEC senescence.

MATERIALS AND METHODS

Lung tissue and primary cultures of AECs

Unless stated otherwise, lung tissue was obtained from patients at the John Hunter Hospital (New Lambton Heights, NSW, Australia) under ethical approval from the human research ethics committees of both the hospital (16/07/20/5.03) and University of Newcastle (H-2016-0325); following guidelines from the National Health and Medical Research Council (NHMRC, Australia). All patients provided written, informed consent for their tissue to be utilised in medical research, and were classified as either IPF or Control (Ctrl). Four primary cultures of IPF-AECs were established from parenchymal tissue of lung obtained from deceased IPF patients 1-2.5 h post-mortem, which were stored in Hank's balanced saline solution (HBSS) at 4^{o}C (between 4-18 h) before cell isolation and culture. The fifth culture of IPF-AECs was established from lung of an IPF patient undergoing lung transplant at St Vincent's Hospital (Sydney, NSW, Australia). Histological staining of lung sections from these IPF patients show extensive pulmonary fibrosis (**Figure S1**, data supplement). For Ctrl-AECs, macroscopically normal parenchymal lung tissue resections were obtained from patients with no evidence of interstitial lung disease (ILD), mostly patients with cancer, undergoing thoracic surgery. Demographic data of patients is provided in **table S1** (data supplement).

AEC cultures were established using parenchymal tissue in a multi-step process involving enzyme digestion, differential cell adhesion and cell sorting. Briefly, tissue (1-10 g) was washed and minced before enzymatic digestion in 30 mL HBSS containing elastase (1.125 U), trypsin (750 U) and collagenase (1875 U) at 37^{o}C for 60 min. The tissue digest was neutralized by addition of an equal volume of Dulbecco's Modified Eagles Medium (DMEM)-Hams F12 medium containing 20% v/v fetal calf serum (FCS) and DNAse I

(15,000 U) before successive passage through 100 and 40 micron cell strainers. Dissociated cells were pelleted by centrifugation before resuspension in adhesion medium comprised of a 1:1 ratio of bronchial epithelial cell growth medium (BEGM, Lonza) and DMEM-Hams F12 with 1% v/v FCS and DNASe I (300 U/mL). Cells were then seeded into T75 flasks, which were kept in an incubator at 37^{o}C for 2 h to allow for macrophage and fibroblast adhesion. Afterwards, unattached cells were removed, washed and resuspended in HBSS before incubation with Anti-CD326 (EpCAM) conjugated magnetic MicroBeads (Miltenyi Biotec) for 30 min to select epithelial cells. The cell suspension was pipetted onto a MiniMACS column (Miltenyi Biotec) attached to a magnet and allowed to flow through the column. After several washes with HBSS, the magnet was removed and the cells that were attached in the magnetic field were eluted into BEGM with 1% v/v FCS, before being seeded into flasks. The culture medium was replenished thereafter every 2-3 days. Flasks typically reached 80-90% confluency within 2-4 weeks of seeding, after which they were sub-cultured.

Cell culture conditions and treatments

Submerged primary cultures of AECs, after the first or second passage, were grown in tissue culture plates in BEGM at 37°C in air containing 5% CO_2. Treatments, including RU.521 (3 μM, Aobious), DNaseI (100 U/mL, Sigma) and ectopic mtDNA (0.1 μg/mL) isolated from human lung fibroblasts were added to the culture medium 24 h after cells were seeded into 6, 12, 24 or 48 well plates (2 x 10^4 cells/cm^2) and re-added with each subsequent medium change (every 2-3 days) over a 7 day period. For etoposide-induced senescence experiments, Ctrl-AECs were treated once with etoposide (10 μM) or the appropriate volume of DMSO as vehicle control. After 24 h incubation with etoposide, the medium was replenished with fresh BEGM. RU.521 was added 30 min before etoposide, and re-added with each subsequent medium change (every 2-3 days) for a total of 5 days after the initial addition of etoposide.

For experiments with the A549 tumor cell line (obtained from ATCC), cells were grown in DMEM containing low glucose (1 g/L), L-alanyl-glutamine (4 mM), sodium pyruvate (1 mM), non-essential amino acids (1% v/v, Sigma) and FCS (1% v/v) at 37°C in air containing 5% CO_2. A549 cells were used between passages 16-21 and treated with etoposide and/or RU.521 as described previously for the primary cultures of AECs. Rotenone (100 nM) or HT-151 (100 nM), inhibitors of complex I of the mitochondrial respiratory chain and STING respectively were also added to A549 cells in selected experiments (12, 31).

siRNA transfection

A549 cells grown in 6 or 24 well plates were transfected with 20 nM RNA siRNA duplex oligonucleotides targeting cGAS using RNA*i*Max Lipofectamine (Invitrogen, CA, USA) according to the manufacturer's instructions. Cells were transfected 24 h after seeding (2 x 10^4 cells/cm^2) in antibiotic-free DMEM containing FCS (10% v/v) by incubation with siRNA-Lipofectamine complex for 4 h. The medium was then replaced with DMEM containing 1% v/v FCS and antibiotics, before cells were maintained for an additional 5 days in culture with subsequent medium changes every 2-3 days. Etoposide was added once, 24 hours following transfection. The sequences of cGAS and control siRNA are provided in Schuliga *et al* (32).

Immunofluorescence detection of cGAS in lung tissue

Lung sections were co-stained for cGAS and epithelial cell adhesion molecule (EpCAM) or p21 by immunofluorescence. Antigens were identified by rabbit polyclonal antibodies to cGAS (#15102, Cell Signaling Technology), -phospho-STING (Ser366) (#19781, Cell Signaling Technology) or p21 (#2947, Cell Signaling Technology) and monoclonal mouse antibodies to EpCAM (#2929, Cell Signaling Technology) or p21 (#6246, Santa Cruz

Biotechnology). Primary antibodies bound to antigen were detected using Alexa Fluor 555 anti-rabbit-conjugate (Cell Signaling Technology) or Alexa Fluor 488 anti-mouse-conjugate (Cell Signaling Technology). All primary antibodies were used at a 1 in 50 dilution, whereas secondary antibodies were used at a 1 in 1000 dilution. Tissues were mounted under coverslips using Prolong Gold AntiFade with DAPI (Molecular Probes, Cell Signaling Technology) and fluorescent images were captured at 200 X magnification using a Nikon Eclipse Ti-U fluorescence microscope.

Immunofluorescence detection of cells in culture

Phosphorylated histone 2AX (H2AXγ), EpCAM, cGAS and surfactant protein A (SP-A) were detected in cells in culture by immunofluorescence. Cells grown in 48-well plates were fixed with 4% w/v formaldehyde in PBS for 10 min before blocking and permeabilization with 0.15% v/v Triton X-100, 10% v/v goat serum and 1% w/v BSA in PBS for 10 min. Cells were then incubated with anti-H2AXγ (Ser139) (#9718, Cell Signaling Technology), -cGAS (#15102, Cell Signaling Technology) or -SP-A (#sc13977, Santa Cruz Biotechnology) rabbit polyclonal IgG or anti-EpCAM (#2929, Cell Signaling Technology) mouse monoclonal IgG overnight at 4^{o}C. After washing, cells were incubated with Alexa Fluor 555 anti-rabbit-conjugate and/or Alexa Fluor 488 anti-mouse-conjugate (Cell Signaling Technology) for 1 h at room temperature. All antibodies were used at a 1 in 300 dilution. Cells were counterstained with DAPI (1 μg/mL, Sigma) and mounted in 70% v/v glycerol. Fluorescent images of cells were taken at 100 X magnification using a Nikon Eclipse inverted Ti-U fluorescence microscope. For H2AXγ quantitation, the fluorescence intensity of the red (H2AXγ) and blue (DAPI) channels for each image were pseudo-colored and merged using Fiji software (NIH). Quantitation was achieved using macro plugins to specifically measure the percentage area of nucleus associated with fluorescence from H2AXγ.

Immunohistochemistry (IHC)

Serial sections of parenchymal lung tissue from IPF patients embedded in paraffin were immunohistochemically stained for cGAS, p21 and EpCAM. Antigens were identified by rabbit polyclonal antibodies to cGAS (#15102, Cell Signaling Technology), p21 (#2947, Cell Signaling Technology) or EpCAM (#15102, Cell Signaling Technology). Antibody staining was completed using the Dako EnVision anti-rabbit kit as appropriate (Dako Corp., Carpinteria, CA, USA) and 3,3'-diaminobenzidine (Sigma-Aldrich, St Louis, MO, USA); where sections were counterstained with hematoxylin.

Purification of mtDNA

Primary cultures of human lung fibroblasts established as previously described and grown to confluence in T75 tissue culture flasks were harvested by trypsinization (32). Mitochondria were isolated using the Mitochondrial Isolation Kit for Cultured Cells (ThermoScientific) according to the Manufacturer's instruction. DNA was extracted from mitochondria using QIAamp DNA mini spin columns (Qiagen). mtDNA was isolated from fibroblasts rather than epithelial cells because high numbers of cells were required to isolate enough mtDNA for experimentation.

Senescence-associated β-galactosidase detection

For senescence-associated β-galactosidase (SA-β-Gal) staining, cell cultures in 12 or 24 well plates were fixed and stained using a commercial kit (Cell Signaling Technology) according to the manufacturer's instructions. Cells were imaged using an Olympus IX51 inverted microscope. SA-β-Gal staining was used qualitatively in the assessment of senescence, with images being representative of 2-3 separate experiments.

Preparation of cytosol extracts

Cells were harvested by trypsinization before resuspension in 1mL PBS. The cells in 900 µL suspension were pelleted by centrifugation (300 *g*) before sub-cellular fractionation using the Mitochondrial Isolation Kit for Cultured Cells (ThermoScientific) according to the Manufacturer's instruction. The kit allows for the isolation of a cytosol fraction free of nuclei and mitochondria (32). The remaining 100 µL of cell suspension was combined with 700 µL of 50 µM NaOH before heating at 100^{o}C for 30 min, then neutralization by the addition of 200 µL 1M Tris-HCl pH 8. Denatured whole cell extracts allow levels of mtDNA detected in the cytosol fraction (and medium) to be normalized to total mtDNA in the cells.

ELISA

Levels of IL-6, interferon-β (IFN-β) and transforming growth factor-β1 (TGF-β1) in conditioned medium were measured by specific sandwich enzyme-linked immunosorbent assays (ELISA) using commercial kits (DuoSets, RnDSystems, MN, USA) as according to the manufacturer's instructions.

PCR analysis

Levels of nucleic acids were analyzed by real time polymerase chain reaction (PCR). RNA and DNA were purified from cells and/or from subcellular fractions (ie cytosol and conditioned media) using RNeasy and QIAamp DNA mini spin columns (Qiagen) respectively. RNA was reverse transcribed into cDNA using the iScript Advanced cDNA kit (BioRad). DNA was amplified by qPCR using the iTaq Universal SYBR Green Supermix (BioRad) in an ABI Prism 7500HT sequence detection system (Applied Biosystems) with the relevant PCR primers (sequences provided in Schuliga *et al* (32)). For RNA quantitation, the

threshold cycle (CT) value determined for each gene of each sample was normalized against that obtained for 18S rRNA, used as an internal control. The level of mRNA for a particular gene is proportional to $2^{-(\Delta CT)}$, where ΔCT is the difference between the CT values of the target gene and 18S rRNA. Relative levels (2^{-CT}) of mtDNA and nuclear DNA (nDNA) in the cytosol fraction and media were measured using PCR primers for the mitochondrial and nuclear genes, $tRNA^{Leu(UUR)}$ and β2-microglobulin (B2M) respectively, expressed as a percentage of their levels detected in denatured whole cell extracts.

Statistical analysis

Grouped data are graphed as box and whisker plots. For experiments with primary cultures, *n* represents individual experiments conducted using AECs from separate IPF patients or controls. For A549 cells, two separate experiments with three biological replicates per treatment group per experiment were conducted. Comparisons between two groups were analyzed by the non-parametric Wilcoxon matched pairs signed rank or Mann-Whitney U tests (Graphpad Prism 5.0, Graphpad, San Diego, CA) as appropriate. A value of $P<0.05$ was considered to be statistically significant.

RESULTS

cGAS is associated with senescent epithelial cells in the fibrotic lung of IPF patients

Immunofluorescence (IF) detection of cGAS in serial sections of lung parenchymal tissue from three separate IPF patients shows cGAS is localized within cells that are positive for the epithelial marker, EpCAM (**Fig. 1** & **Fig. S2**, data supplement). cGAS was also detected in EpCAM positive epithelial cells of lung parenchyma from control donors, albeit expression appeared less intense than in IPF lung (**Fig. 1a)**. Dual-labelling IF of serial sections suggests that cGAS positive regions of epithelium in IPF lung also express phosphorylated STING (pSTING), the downstream mediator of DNA-bound cGAS, and the senescence marker, p21 (**Fig. 1b & 1c**). Although some non-specific fluorescence (green channel) was detected in the staining controls, this fluorescence was extracellular and attributable to auto-fluorescence from ECM protein (**Fig. 1**). Immunohistochemistry of serial sections of lung tissue from an IPF patient provides additional evidence that cGAS and p21 are present within the same populations of epithelial cells (**Fig. 2**).

AECs from IPF patients exhibit high baseline senescence in vitro

Submerged cultures of IPF- and control (Ctrl)-AECs contained EpCAM positive cells, with >85% also exhibiting a pericellular distribution of SP-A, signifying type 2 pneumocytes (AEC2s) (**Fig. 3a-b**). Larger $EpCAM^{+}$, $SP\text{-}A^{-}$ cells were likely to be type I pneumocytes (AEC1s). IPF-AECs (n=5) exhibited a higher baseline senescence than Ctrl-AECs (n=5-7), as measured by increased levels of nuclear H2AXγ, p21 mRNA and production of IL-6 and interferon-β (IFN-β) ($P<0.05$) (**Fig. 3c-f**). The levels of mRNA encoding IL-6 and two other SASP cytokines, CCL2 and IL-8 were also higher in IPF- than Ctrl-AECs (**Fig. S3**, data supplement). Furthermore, SA-β-Gal staining appeared more intense for IPF-AECs, when compared to Ctrl-AECs (**Fig. 3g**).

294

295 *Pharmacological cGAS inhibition diminishes IPF-AEC senescence*

296 Pharmacological cGAS inhibition with RU.521 diminished IPF-AEC senescence in culture
297 for 7 d. The exposure of IPF-AECs from five separate patients during exponential growth to
298 RU.521 reduced the following markers of senescence: levels of nuclear H2AXγ, p21 mRNA,
299 and IL-6 and IFN-β protein (**Fig. 4a-d**). The levels of mRNA transcripts for SASP mediators
300 (IL-6, CCL2 and IL-8) were also lower when compared to the vehicle control (**Fig. S4,** data
301 supplement). Cytochemical staining also suggested that RU.521 reduced the levels of SA-β-
302 Gal (**Fig. 4e**).

303

304 *cGAS drives DNA damage-induced AEC senescence*

305 The role of cGAS in the acquisition of AEC senescence was also examined using Ctrl-AECs.
306 This phenotype exhibited heightened senescence following treatment with the DNA
307 damaging agent, etoposide (10 μM); in a manner sensitive to pharmacological cGAS
308 inhibition using RU.521 (**Fig. 5** & **Fig. S5** data supplement) ($P<0.05$, n=5-6). Comparable
309 effects of RU.521 were observed in cultures of the AEC2 cell line, A549 following treatment
310 with etoposide (**Fig. S6** data supplement) ($P<0.05$, n=5-6). Additionally, transfection of A549
311 cells with cGAS-selective siRNA attenuated etoposide-induced increases in senescent
312 markers (**Fig. 6** & **Fig. S7** online supplement) ($P<0.05$, n=5-6). Furthermore, the
313 pharmacological inhibition of STING in A549 cells using HT-151 (0.1 μM) also attenuated
314 etoposide-induced increases in senescence markers (**Fig. S8,** data supplement) ($P<0.05$, n=6-
315 7).

316

317 *mtDNA release is higher in senescent AECs*

The release of mtDNA and nuclear DNA (nDNA) by AECs were assessed by qPCR using primers for $tRNA^{Leu(UUR)}$ and β2-microglobulin (B2M), respectively (28). Levels of mtDNA in the cytosol and conditioned medium (CM) of IPF-AECs (expressed as % of total cellular mtDNA) were higher than Ctrl-AECs (**Fig. 7a**) ($P<0.05$, n=5-6). Etoposide-induced Ctrl-AEC senescence corresponded with an increase in the release of mtDNA into the cytosol and extracellular space (**Fig. 7b**) ($P<0.05$, n=6). Levels of nDNA were also higher in the CM of IPF-AECs and senescence-induced Ctrl-AECs when compared to baseline levels of Ctrl-AECs (**Fig. 7c-d**) ($P<0.05$, n=5-6). However, no differences in the levels of nDNA in the cytosolic fractions were observed ($P>0.05$, n=5-6).

Rotenone induces mtDNA release and AEC senescence in a cGAS-dependent manner

Increased levels of mtDNA in the cytosol of IPF- and etoposide-treated Ctrl-AECs suggests mtDNA damage and release contributes to the senescence phenotype. To delineate the specific contribution of endogenous mtDNA in cGAS activation and senescence, AECs cells were treated with rotenone; an inducer of mitochondrial stress and subsequent mtDNA damage (31). Incubation of A549 cells with rotenone (100 nM) evoked mtDNA release as shown by increases in the levels of mtDNA detected in both the cytosol and supernatant (**Fig. 8a**) ($P<0.05$, n=6). Such increases corresponded with increases in markers of senescence including increased levels of nuclear H2AXγ, p21 mRNA and IL-6, IFN-β and TGF-β cytokine production (**Fig. 8b-f**) ($P<0.05$, n=5-7). These rotenone-induced increases were sensitive to cGAS inhibition using RU.521 (**Fig. 8b-f**) ($P<0.05$, n=5-7).

Extracellular DNA augments AEC senescence in a cGAS-dependent manner

We next examined whether extracellular DNA contributes to AEC senescence. The addition of the endonuclease, DNAse I (100 U/mL, 7d) reduced the levels of all senescence markers,

except CCL2 mRNA, evaluated in cultures of IPF-AECs from 5 separate donors ($P<0.05$, $n=5$); suggesting that increased levels of extracellular self-DNA may mediate secondary senescence in autocrine and/or paracrine manners (**Fig. 9** & **Fig. S9** data supplement). Furthermore, mtDNA derived from human lung fibroblasts and added to the medium of Ctrl-AECs induced increases in senescent markers, including p21 expression (**Fig. 10** & **Fig. S10** data supplement) ($P<0.05$, $n=5$). The effect of ectopic mtDNA on Ctrl-AEC senescence was sensitive to cGAS inhibition using RU.521 ($P<0.05$, $n=5$).

DISCUSSION

This study examined the roles of self-DNA and cGAS in AEC senescence, a feature of IPF pathology (14, 19, 23, 33). cGAS and pSTING were detected in epithelial cells of lung parenchymal sections from IPF patients, including cells positive for the senescent marker, p21. Using submerged primary cultures of AECs comprised predominantly of AEC2s, IPF-AECs were shown to release higher levels of mtDNA into the cytosolic- and extracellular-spaces than Ctrl-AECs and this corresponded to higher baseline senescence. Increased levels of mtDNA detected in the cytosol and conditioned medium of Ctrl-AECs following treatment with etoposide provides additional evidence that increased mtDNA release is a feature of AEC senescence. Pharmacological inhibition of cGAS in IPF-AECs *in vitro* diminished senescence, implicating cGAS as a sensor of cytosolic damaged DNA in AEC senescence. In support, targeting cGAS attenuated etoposide-induced Ctrl-AEC and A549 senescence. Additionally, pharmacological STING inhibition also attenuated etoposide-induced A549 senescence. Furthermore, ectopic mtDNA augmented Ctrl-AEC senscence in a cGAS-dependent manner and DNAseI attenuated IPF-AEC senescence, suggesting a contribution of extracellular DNA to autocrine and/or paracrine senescence. Collectively, our data indicates that a cGAS-dependent response links DNA damage and AEC senescence in IPF. Our findings are potentially important, particularly as AEC senescence is proposed to be the crux of the aberrant wound healing response of IPF; possibly by hindering re-epithelialization and/or by the activation of resident fibroblasts (8).

Cytosolic cGAS binds dsDNA irrespective of sequence to generate cGAMP and a subsequent inflammatory/interferon-like response via the activation of the STING pathway. Asides from its role in innate immunity, cGAS is an essential mediator of damaged DNA-induced cellular senescence (11, 42). Whilst there is accumulating evidence that AEC senescence is crucial in

IPF pathology, little is known about the underlying contributions of self-DNA and/or cGAS to this cellular process. In the current study, cGAS antigen was detected in epithelial cells of lung parenchymal tissue from IPF patients. cGAS immunoreactivity in epithelial cells of fibrotic lung appeared to be more intense than in parenchymal lung tissue from control donors. cGAS was also detected in senescent (p21 expressing) epithelial cells in IPF lung. Targeting cGAS using RU.521 diminished IPF-AEC senescence *in vitro* and attenuated etoposide-induced Ctrl-AEC senescence as assessed by concomitant decreases in a range of parameters widely used in the evaluation of cellular senescence (11, 19, 31, 41, 42). One of those markers, H2AXγ is a surrogate of nuclear DNA damage, being phosphorylated at dsDNA breaks in the nucleus as part of the DNA damage response (DDR) that initiates senescence (31). It is likely that the effects of targeting cGAS on AEC senescence involves the attenuation of NF-κB-regulated SASP cytokine expression. NF-κB is activated downstream of the STING signaling pathway and is a pivotal regulator of the SASP secretome (11). The latter comprises an array of cytokines, chemokines and proteases that can mediate secondary senescence via autocrine and paracrine processes. In this study, the impact of targeting cGAS on the SASP was evidenced by decreases in the production of IL-6 (the archetypal SASP cytokine), TGF-β and expression of the IL-6, CCL2 and IL-8 genes in primary AECs and/or A549s. However, other SASP mediators were not analysed in this study, nor was the causal involvement of NF-κB in regulating the SASP and secondary senescence. Despite these shortcomings, our current data provides evidence that cGAS is an important mediator of AEC senescence, with a potential role in IPF pathology.

The sequential activation of TANK-binding kinase-1 (TBK1) and interferon regulatory factor-3 (IRF3), downstream mediators of STING, leads to the induction of interferon I and III gene expression. In this study, levels of the type I interferon, IFN-β were also increased in

403 the medium of senescent AECs in a cGAS-dependent manner. However, a causal role of
404 IFN-β in mediating AEC senescence was not evaluated. Whilst IFN-β is not a universal
405 component of the SASP (nor are most SASP components), there is growing evidence that
406 type I interferons contribute to cellular senescence. For example, prolonged treatment of
407 fibroblasts with IFN-β induces nuclear DNA damage and a subsequent DDR leading to
408 senescence (34). However, the mechanisms by which IFN-β and other type I interferons may
409 evoke cellular senescence is not yet well understood (10).
410
411 Damage to mtDNA such as base oxidation and deletions increases in frequency with
412 oxidative stress and accumulates in ageing and diseased tissue (17). These modifications
413 reduce the physical association of mtDNA with mitochondrial packaging proteins, leading to
414 the leakage of mtDNA and its accumulation in the cytosol (39). Other mechanisms may also
415 contribute to increases in cytosolic mtDNA including diminished mitophagy, as observed in
416 primary cultures of AEC2s derived from IPF patients, and AEC2s of control donors/A549
417 cells subject to ER and oxidative stress (6). Cytosolic self-DNA, whether of mitochondrial or
418 nuclear origin, elicits cGAS-dependent cell-autonomous inflammatory responses (ie sterile
419 inflammation) (1, 40). Recently, Han *et al* reported that cytosolic levels of self dsDNA in the
420 airway epithelium of mice are elevated following challenge with allergen and that cGAS
421 knockout specifically in airway epithelial cells attenuates allergen-induced airway
422 inflammation (13). Furthermore, the targeting of cGAS and/or STING has been shown to
423 attenuate lung inflammation induced by acute exposure to either cigarette smoke (CS) or
424 silica microparticles (3, 24). However, a recent study using the murine bleomycin lung
425 fibrosis model, showed that whilst bleomycin evoked increases in the extracellular release of
426 self DNA and expression of STING and cGAS in the lungs, STING gene deletion augmented
427 fibrosis (30). This effect of STING, which was independent of cGAS and IFN I/III expression

was mediated by a dysregulated immune response involving exacerbated neutrophilic inflammation. This immunomodulatory effect of STING potentially involves alternative pathways mediated by DNA sensors such as DDX41 and IFI16, including a recently identified non-canonical, cGAS-independent pathway that leads to prominent NF-κB activation, but only modest IRF3 expression (9, 43).

As mentioned previously, innate immune sensing of cytosolic DNA by cGAS also promotes senescence. Whilst earlier studies have implicated damaged nuclear DNA (nDNA) as an activator of cGAS-dependent senescence, it is likely that mtDNA contributes as well (11, 41, 42). Our data that shows increased levels of mtDNA in both the cytosol and extracellular space of senescent AECs implicates mtDNA as a potential driver of IPF-AEC senescence. To provide additional evidence that mitochondrial dysfunction is the underlying cause of mtDNA release in AEC, we induced mitochondrial stress in A549 cells using rotenone, an agent that targets complex I of the inner mitochondrial membrane to induce superoxide formation. Rotenone not only induced an increase in the release of mtDNA, but also senescence in a manner sensitive to cGAS inhibition. Furthermore, ectopic mtDNA was shown to induce AEC senescence in a cGAS-dependent manner. We should also make note, that levels of nDNA were also increased in the medium, albeit not cytosol of IPF-AECs and etoposide-treated Ctrl-AECs when compared to Ctrl-AECs at baseline. It is plausible and highly likely that nDNA may also contribute to AEC senescence involving cGAS. Collectively our data support a contribution of self-DNA in AEC senescence involving cGAS. The involvement of other PRRs such as TLR9 or absent in melanoma 2 (AIM2) were not assessed in this study.

Previous investigations with AECs from IPF patients have shown that they are prone to both senescence and mitochondrial dysfunction (6-8, 19, 23). Our studies with lung fibroblasts, including those from IPF patients (ie IPF-LFs) provide evidence that both processes are linked as part of a viscous circle involving increased production of mitochondrial-derived ROS (5, 31, 38). Our recent findings with IPF-LFs and current data with IPF-AECs also identify mtDNA and cGAS as potential mediators of senescence. We propose that in IPF, damaged mtDNA leaked into the cytoplasmic and extracellular spaces of AECs by aging, dysfunctional mitochondria activates cytosolic cGAS to evoke a 'sterile' inflammatory response that perpetuates secondary senescence (**Fig. 11**). Senescent AECs do not self-renew following injury but produce more cytokines in a failed attempt to re-epithelialize. The spill over of SASP mediators by senescent AECs may contribute to a fibrotic niche that influences neighboring lung fibroblasts, including their transition into a senescence phenotype (*ie* the bystander effect' (25)). In support, the culture of 'naïve' human lung fibroblasts with conditioned medium from senescent AECs induces senescence in the former (Waters *et al*, In press). Interestingly, lung fibroblast senescence is also associated with increased expression of α-smooth muscle actin and collagen type I alpha, markers of the myofibroblast phenotype (31, 41). The bioactive molecules that mediate the transfer of senescence from AECs to lung fibroblasts and/or their activation is yet to be determined, but could involve ROS, cytokines (ie IL-6), growth factors (ie TGF-β) and/or DAMPs including mtDNA (4, 26, 31, 32). Indeed, Bueno *et al* recently showed that mtDNA induces TGF-β release in primary human lung epithelial cells as well as activation of human lung fibroblasts, as measured by increased expression of α-smooth muscle actin (7). Overall, our current findings have added significance in understanding IPF pathology following the recent discovery that higher levels of extracellular mtDNA occur in IPF and are predictive of all-cause mortality (29).

Targeting cGAS-STING signalling may be a potential treatment option for IPF because AEC senescence is thought to contribute to the aberrant wound repair response that drives fibrosis (33). Whilst RU.521 is a highly selective cGAS inhibitor, its potency is substantially diminished for DNA substrates of shorter length (<100 bp), possibly limiting its therapeutic potential *in vivo* (18, 21, 36, 44). The recent discovery of small molecular drugs with improved efficacy for inhibiting human cGAS activated by shorter DNA substrates, provides greater opportunity for the clinical use of pharmacological cGAS inhibitors (18). Other drugs such as the recently discovered highly selective inhibitor of STING, H-151 may also have therapeutic potential, as would agents that preserve mtDNA integrity (ie MitoTEMPO) or recombinant DNAses that target cell free DNA (12, 35). Further exploration of pharmacological cGAS-STING signalling pathway inhibitors and ectopic DNAses in pre-clinical models of lung fibrosis is clearly warranted.

In conclusion, we show that cGAS inhibition diminishes IPF-AEC senescence and chemical-induced Ctrl-AEC senescence. We also provide evidence that AEC senescence is associated with an increase in the release of DNA, which reinforces senescence in a cGAS-dependent manner. Overall, our study suggests that damaged, self-DNA activates cGAS to perpetuate AEC senescence and aging in IPF and other fibrotic lung diseases. We propose that cGAS is potentially a central player in IPF pathology; connecting mitochondrial stress, sterile inflammation (involving cGAS activation by self-DNA) and senescence.

ACKNOWLEDGEMENTS

This work was supported by the NHMRC (Australia) research grant #1099569. JK Burgess was supported by a Rosalind Franklin Fellowship from the University of Groningen and the European Union. We thank the patients, thoracic surgeons, respiratory clinicians, pathologists and medical staff at the John Hunter Hospital (Newcastle) and St Vincent's Hospital (Sydney) for assistance in obtaining expertly phenotyped human lung tissue.

AUTHORS CONTRIBUTION Concept and design: DAK, MS; acquisition, analysis and interpretation of data: MS, AK, JR, CT, CG, KECB, AJ; and drafting the manuscript for intellectual content: DAK, MS, CG, JKB, CMP, SEM and NB.

CONFLICTS OF INTEREST

The authors confirm that there are no conflicts of interest.

REFERENCES

1. **Aarreberg LD, Esser-Nobis K, Driscoll C, Shuvarikov A, Roby JA, and Gale M, Jr.** Interleukin-1beta Induces mtDNA Release to Activate Innate Immune Signaling via cGAS-STING. *Mol Cell* 2019.
2. **Armanios MY, Chen JJ, Cogan JD, Alder JK, Ingersoll RG, Markin C, Lawson WE, Xie M, Vulto I, Phillips JA, 3rd, Lansdorp PM, Greider CW, and Loyd JE**. Telomerase mutations in families with idiopathic pulmonary fibrosis. *N Engl J Med* 356: 1317-1326, 2007.
3. **Benmerzoug S, Rose S, Bounab B, Gosset D, Duneau L, Chenuet P, Mollet L, Le Bert M, Lambers C, Geleff S, Roth M, Fauconnier L, Sedda D, Carvalho C, Perche O, Laurenceau D, Ryffel B, Apetoh L, Kiziltunc A, Uslu H, Albez FS, Akgun M, Togbe D, and Quesniaux VFJ**. STING-dependent sensing of self-DNA drives silica-induced lung inflammation. *Nat Commun* 9: 5226, 2018.
4. **Blokland KEC, Pouwels SD, Schuliga M, Knight DA, and Burgess JK**. Regulation of cellular senescence by extracellular matrix during chronic fibrotic diseases. *Clin Sci (Lond)* 134: 2681-2706, 2020.
5. **Blokland KEC, Waters DW, Schuliga M, Read J, Pouwels SD, Grainge CL, Jaffar J, Westall G, Mutsaers SE, Prêle CM, Burgess JK, and Knight DA**. Senescence of IPF Lung Fibroblasts Disrupt Alveolar Epithelial Cell Proliferation and Promote Migration in Wound Healing. *Pharmaceutics* 12: 2020.
6. **Bueno M, Lai YC, Romero Y, Brands J, St Croix CM, Kamga C, Corey C, Herazo-Maya JD, Sembrat J, Lee JS, Duncan SR, Rojas M, Shiva S, Chu CT, and Mora AL**. PINK1 deficiency impairs mitochondrial homeostasis and promotes lung fibrosis. *J Clin Invest* 125: 521-538, 2015.
7. **Bueno M, Zank D, Buendia-Roldan I, Fiedler K, Mays BG, Alvarez D, Sembrat J, Kimball B, Bullock JK, Martin JL, Nouraie M, Kaufman BA, Rojas M, Pardo A, Selman M, and Mora AL**. PINK1 attenuates mtDNA release in alveolar epithelial cells and TLR9 mediated profibrotic responses. *PLoS One* 14: e0218003, 2019.
8. **Chilosi M, Carloni A, Rossi A, and Poletti V**. Premature lung aging and cellular senescence in the pathogenesis of idiopathic pulmonary fibrosis and COPD/emphysema. *Transl Res* 162: 156-173, 2013.
9. **Dunphy G, Flannery SM, Almine JF, Connolly DJ, Paulus C, Jonsson KL, Jakobsen MR, Nevels MM, Bowie AG, and Unterholzner L**. Non-canonical Activation of the DNA Sensing Adaptor STING by ATM and IFI16 Mediates NF-kappaB Signaling after Nuclear DNA Damage. *Mol Cell* 71: 745-760 e745, 2018.
10. **Frisch SM, and MacFawn IP**. Type I interferons and related pathways in cell senescence. *Aging Cell* 19: e13234, 2020.
11. **Gluck S, Guey B, Gulen MF, Wolter K, Kang TW, Schmacke NA, Bridgeman A, Rehwinkel J, Zender L, and Ablasser A**. Innate immune sensing of cytosolic chromatin fragments through cGAS promotes senescence. *Nat Cell Biol* 19: 1061-1070, 2017.
12. **Haag SM, Gulen MF, Reymond L, Gibelin A, Abrami L, Decout A, Heymann M, van der Goot FG, Turcatti G, Behrendt R, and Ablasser A**. Targeting STING with covalent small-molecule inhibitors. *Nature* 559: 269-273, 2018.
13. **Han Y, Chen L, Liu H, Jin Z, Wu Y, Wu Y, Li W, Ying S, Chen Z, Shen H, and Yan F**. Airway Epithelial cGAS Is Critical for Induction of Experimental Allergic Airway Inflammation. *J Immunol* 204: 1437-1447, 2020.
14. **Hecker L, Logsdon NJ, Kurundkar D, Kurundkar A, Bernard K, Hock T, Meldrum E, Sanders YY, and Thannickal VJ**. Reversal of persistent fibrosis in aging by targeting Nox4-Nrf2 redox imbalance. *Sci Transl Med* 6: 231ra247, 2014.
15. **Kim SJ, Cheresh P, Jablonski RP, Williams DB, and Kamp DW**. The Role of Mitochondrial DNA in Mediating Alveolar Epithelial Cell Apoptosis and Pulmonary Fibrosis. *Int J Mol Sci* 16: 21486-21519, 2015.
16. **Korolchuk VI, Miwa S, Carroll B, and von Zglinicki T**. Mitochondria in Cell Senescence: Is Mitophagy the Weakest Link? *EBioMedicine* 21: 7-13, 2017.

17. **Lal A, Gomez E, and Calloway C**. Increased mitochondrial DNA deletions and copy number in transfusion-dependent thalassemia. *JCI Insight* 1: 2016.
18. **Lama L, Adura C, Xie W, Tomita D, Kamei T, Kuryavyi V, Gogakos T, Steinberg JI, Miller M, Ramos-Espiritu L, Asano Y, Hashizume S, Aida J, Imaeda T, Okamoto R, Jennings AJ, Michino M, Kuroita T, Stamford A, Gao P, Meinke P, Glickman JF, Patel DJ, and Tuschl T**. Development of human cGAS-specific small-molecule inhibitors for repression of dsDNA-triggered interferon expression. *Nat Commun* 10: 2261, 2019.
19. **Lehmann M, Korfei M, Mutze K, Klee S, Skronska-Wasek W, Alsafadi HN, Ota C, Costa R, Schiller HB, Lindner M, Wagner DE, Gunther A, and Konigshoff M**. Senolytic drugs target alveolar epithelial cell function and attenuate experimental lung fibrosis ex vivo. *Eur Respir J* 50: 2017.
20. **Ma R, Ortiz Serrano TP, Davis J, Prigge AD, and Ridge KM**. The cGAS-STING pathway: The role of self-DNA sensing in inflammatory lung disease. *FASEB J* 2020.
21. **McLemore A, Hou H-A, Ward G, Onimus A, Vincelette N, Rodrigues M, Chaudhary N, Zhang L, Meyer B, Eksioglu E, Wei S, and List A**. Genomic-DNA Exposed By Somatic Gene Mutations Engages the cGAS/STING Axis to License the NLRP3 Inflammasome in Myelodysplastic Syndromes. *Blood* 132: 3075-3075, 2018.
22. **Murtha LA, Morten M, Schuliga MJ, Mabotuwana NS, Hardy SA, Waters DW, Burgess JK, Ngo DT, Sverdlov AL, Knight DA, and Boyle AJ**. The Role of Pathological Aging in Cardiac and Pulmonary Fibrosis. *Aging and disease* 10: 419-428, 2019.
23. **Naikawadi RP, Disayabutr S, Mallavia B, Donne ML, Green G, La JL, Rock JR, Looney MR, and Wolters PJ**. Telomere dysfunction in alveolar epithelial cells causes lung remodeling and fibrosis. *JCI Insight* 1: e86704, 2016.
24. **Nascimento M, Gombault A, Lacerda-Queiroz N, Panek C, Savigny F, Sbeity M, Bourinet M, Le Bert M, Riteau N, Ryffel B, Quesniaux VFJ, and Couillin I**. Self-DNA release and STING-dependent sensing drives inflammation to cigarette smoke in mice. *Sci Rep* 9: 14848, 2019.
25. **Nelson G, Kucheryavenko O, Wordsworth J, and von Zglinicki T**. The senescent bystander effect is caused by ROS-activated NF-kappaB signalling. *Mech Ageing Dev* 2017.
26. **Nelson G, Wordsworth J, Wang C, Jurk D, Lawless C, Martin-Ruiz C, and von Zglinicki T**. A senescent cell bystander effect: senescence-induced senescence. *Aging cell* 11: 345-349, 2012.
27. **Richeldi L, Collard HR, and Jones MG**. Idiopathic pulmonary fibrosis. *Lancet* 389: 1941-1952, 2017.
28. **Rooney JP, Ryde IT, Sanders LH, Howlett EH, Colton MD, Germ KE, Mayer GD, Greenamyre JT, and Meyer JN**. PCR based determination of mitochondrial DNA copy number in multiple species. *Methods Mol Biol* 1241: 23-38, 2015.
29. **Ryu C, Sun H, Gulati M, Herazo-Maya J, Chen Y, Osafo-Addo A, Brandsdorfer C, Winkler J, Blaul C, Faunce J, Pan H, Woolard T, Tzouvelekis A, Antin-Ozerkis DE, Puchalski JT, Slade M, Gonzalez AL, Bogenhagen DF, Kirillov V, Feghali-Bostwick C, Gibson K, Lindell K, Herzog RI, Dela Cruz CS, Mehal W, Kaminski N, Herzog EL, and Trujillo G**. Extracellular Mitochondrial DNA is Generated by Fibroblasts and Predicts Death in Idiopathic Pulmonary Fibrosis. *Am J Respir Crit Care Med* 2017.
30. **Savigny F, Schricke C, Lacerda-Queiroz N, Meda M, Nascimento M, Huot-Marchand S, Da Gama Monteiro F, Ryffel B, Gombault A, Le Bert M, Couillin I, and Riteau N**. Protective Role of the Nucleic Acid Sensor STING in Pulmonary Fibrosis. *Front Immunol* 11: 588799, 2020.
31. **Schuliga M, Pechkovsky DV, Read J, Waters DW, Blokland KEC, Reid AT, Hogaboam CM, Khalil N, Burgess JK, Prele CM, Mutsaers SE, Jaffar J, Westall G, Grainge C, and Knight DA**. Mitochondrial dysfunction contributes to the senescent phenotype of IPF lung fibroblasts. *J Cell Mol Med* 22: 5847-5861, 2018.
32. **Schuliga M, Read J, Blokland KE, Waters DW, Burgess J, Prele C, Mutsaers SE, Jaffar J, Westall G, Reid A, James A, Grainge C, and Knight DA**. Self DNA perpetuates IPF lung fibroblast senescence in a cGAS-dependent manner. *Clin Sci (Lond)* 2020.

33. **Schuliga M, Read J, and Knight DA**. Ageing mechanisms that contribute to tissue remodeling in lung disease. *Ageing Res Rev* 70: 101405, 2021.
34. **Takaoka A, Hayakawa S, Yanai H, Stoiber D, Negishi H, Kikuchi H, Sasaki S, Imai K, Shibue T, Honda K, and Taniguchi T**. Integration of interferon-alpha/beta signalling to p53 responses in tumour suppression and antiviral defence. *Nature* 424: 516-523, 2003.
35. **Wang M, Sooreshjani MA, Mikek C, Opoku-Temeng C, and Sintim HO**. Suramin potently inhibits cGAMP synthase, cGAS, in THP1 cells to modulate IFN-beta levels. *Future Med Chem* 10: 1301-1317, 2018.
36. **Wang R, Wang W, Li A, Wang Y, Jin J, Huang Z, and Huang G**. Lipopolysaccharide enhances DNA-induced IFN-beta expression and autophagy by upregulating cGAS expression in A549 cells. *Exp Ther Med* 18: 4157-4164, 2019.
37. **Waters DW, Blokland KEC, Pathinayake PS, Burgess JK, Mutsaers SE, Prele CM, Schuliga M, Grainge CL, and Knight DA**. Fibroblast senescence in the pathology of idiopathic pulmonary fibrosis. *Am J Physiol Lung Cell Mol Physiol* 2018.
38. **Waters DW, Blokland KEC, Pathinayake PS, Wei L, Schuliga M, Jaffar J, Westall GP, Hansbro PM, Prele CM, Mutsaers SE, Bartlett NW, Burgess JK, Grainge CL, and Knight DA**. STAT3 Regulates the Onset of Oxidant-Induced Senescence in Lung Fibroblasts. *Am J Respir Cell Mol Biol* 2019.
39. **West AP, Khoury-Hanold W, Staron M, Tal MC, Pineda CM, Lang SM, Bestwick M, Duguay BA, Raimundo N, MacDuff DA, Kaech SM, Smiley JR, Means RE, Iwasaki A, and Shadel GS**. Mitochondrial DNA stress primes the antiviral innate immune response. *Nature* 520: 553-557, 2015.
40. **West AP, and Shadel GS**. Mitochondrial DNA in innate immune responses and inflammatory pathology. *Nat Rev Immunol* 17: 363-375, 2017.
41. **Yanai H, Shteinberg A, Porat Z, Budovsky A, Braiman A, Ziesche R, and Fraifeld VE**. Cellular senescence-like features of lung fibroblasts derived from idiopathic pulmonary fibrosis patients. *Aging (Albany NY)* 7: 664-672, 2015.
42. **Yang H, Wang H, Ren J, Chen Q, and Chen ZJ**. cGAS is essential for cellular senescence. *Proc Natl Acad Sci U S A* 114: E4612-E4620, 2017.
43. **Zhang Z, Yuan B, Bao M, Lu N, Kim T, and Liu YJ**. The helicase DDX41 senses intracellular DNA mediated by the adaptor STING in dendritic cells. *Nat Immunol* 12: 959-965, 2011.
44. **Zhou W, Whiteley AT, de Oliveira Mann CC, Morehouse BR, Nowak RP, Fischer ES, Gray NS, Mekalanos JJ, and Kranzusch PJ**. Structure of the Human cGAS-DNA Complex Reveals Enhanced Control of Immune Surveillance. *Cell* 174: 300-311 e311, 2018.

FIGURE LEGENDS

Figure 1. *cGAS antigen is detected within senescent epithelial cells of IPF lung.* (**a, top panel**) Sections of lung parenchymal tissue from a patient with IPF (patient 1) and control donor were immunostained for cGAS (red) and EpCAM (green) and counterstained for DAPI (blue). Arrows show cGAS within EpCAM positive cells. (**b, top**) Section of IPF lung (patient A) immunostained for cGAS (red) in combination with p21 (green). Arrows show cGAS and p21 co-localisation in epithelial cells. (**c**) Serial sections of lung from another patient with IPF (patient 3) immunostained for EpCAM (green) in combination with cGAS (red, **top left panel**), p-STING (red, **bottom left panel**) and p21 (red, **top right panel**). (**a-c, bottom (right) panel**) Primary antibodies were omitted in corresponding serial sections designated as staining controls. Scale bar = 50 micron.

Figure 2. *Immunohistochemical detection of cGAS in senescent epithelial cells of IPF lung.* Serial sections from the same region of lung from a patient with IPF (patient 1) stained with hematoxylin (blue/purple) and cGAS (brown, **top left panel**), EpCAM (brown, **top right panel**) and p21 (brown, **bottom left panel**). Primary antibodies were omitted in corresponding serial section designated as staining control (**bottom right label**). Scale bar = 50 micro*n.*

Figure 3. *IPF-AECs exhibit high baseline senescence.* (**a-b**) Immunofluorescence and phase-contrast images of submerged primary cultures of Ctrl-AECs (**a-b**) and IPF-AECs (**b**). Cells were immunostained for EpCAM (green) and SP-A (red). (**c-f**) The senescence of IPF-AECS (n=5) and Ctrl-AECs (n=5-6) at baseline was assessed by measuring levels of nuclear H2AXγ (with representative fluorescence images) (**c**), p21 mRNA (**d**) and IL-6 (**e**) and IFN-β (**f**) protein. (**g**) Representative images of SA-β-Gal cytochemical stains of IPF and Ctrl-

673 AECs. Quantitative data were analyzed by a Mann Whitney test (*P<0.05). Scale bar = 50
674 micron.
675
676 **Figure 4.** *Targeting cGAS diminishes IPF-AEC senescence.* (**a-e**) The effect of RU.521 (3
677 μM) on the senescence phenotype of IPF-AECs (n=5) after 7 d, as measured by changes in
678 the levels of nuclear H2AXγ (a), p21 mRNA (b) and IL-6 (c) and IFN-β (d) protein. Included
679 are representative images of H2AXγ immunofluorescence (b) and SA-β-Gal cytochemical
680 staining (e). Differences between vehicle and treatment groups were assessed by a Wilcoxon
681 matched pairs signed rank test (*P<0.05, n=5). Scale bar = 50 micron.
682
683 **Figure 5.** *cGAS inhibition attenuates etoposide-induced Ctrl-AEC senescence.* (**a-e**) The
684 effect of RU.521 (3 μM) on the senescence phenotype of Ctrl-AECs 5 d after the addition of
685 etoposide (10 μM). Included are representative fluorescence images of H2AXγ and
686 cytochemical staining for SA-β-Gal. Data were analyzed by Friedman's analysis of variance
687 (ANOVA) with differences between two treatment groups assessed by a Wilcoxon matched
688 pairs signed rank test (*P<0.05, n=5-6). Scale bar = 50 micron.
689
690 **Figure 6.** *cGAS knockdown attenuates A549 senescence.* (**a**) Levels of cGAS mRNA
691 (*P<0.05, n=5) and immunoreactivity (images representative of three replicates) in A549
692 cells, 1 d post siRNA transfection. (**b-f**) The effect of cGAS siRNA on A549 senescence 5 d
693 after addition of etoposide. Quantitative data were analyzed by Friedman's ANOVA with
694 differences between two treatment groups assessed by a Wilcoxon matched pairs signed rank
695 test (*P<0.05, n=5). Scale bar = 50 micron.
696

Figure 7. *IPF- and senescent-induced Ctrl-AECs release increased amounts of mtDNA.* (**a**) Baseline levels of mtDNA in the cytosol and medium of IPF- and Ctrl-AECs as detected by qPCR using primers for the mitochondrial gene, mt-tRNAleu$_{(UUR)}$. Levels of mtDNA are expressed as a percentage of total mtDNA detected in cells. Data were analyzed by a Mann Whitney test (*P<0.05, n=5-6). (**b**) Levels of mtDNA in the cytosol and medium of etoposide-treated Ctrl-AECs (10 μM, 3 d). Differences between two treatment groups were analyzed by a Wilcoxon matched pairs signed rank test (*P<0.05, n=6). (**c, d**) Levels of nDNA, as detected using primers for B2M in the cytosol and media of IPF- and Ctrl-AECs at baseline, and etoposide-treated Ctrl-AECs (*P<0.05, n=5-6).

Figure 8. *Targeting cGAS attenuates rotenone-induced A549 senescence.* (**a**) Levels of mtDNA in the cytosol and medium of rotenone-treated A549 cells (0.1 μM, 2 d). (**b-f**) The effect of RU.521 (3 μM) on the senescence phenotype of rotenone-treated cells after 5 d, as measured by changes in the levels of nuclear γH2AX, p21 mRNA and IL-6, IFN-β and TGF-β protein in conditioned media. Differences between two treatment groups were analyzed by a Mann Whitney test, *P<0.05 (n=5-6). Scale bar in images = 50 micron.

Figure 9. *DNAseI diminishes the escalation of IPF-AEC senescence.* **(a-e)** IPF-AECs (n=5) in culture treated with DNAseI (50 U) for 7 d were evaluated for markers of senescence, including levels of nuclear γH2AX (a), p21 mRNA (b), and IL-6 (c) and IFN-β (d) protein . Representative fluorescence images of γH2AX and cytochemical staining for SA-β-Gal (e) are shown. Scale bar = 50 micron.

Figure 10. *Ectopic mtDNA induces Ctrl-AEC senescence in a cGAS-dependent manner.* **(a-e)** The combined effects of ectopic mtDNA (0.1 μg/mL) and RU.521 (3 μM) on Ctrl-LF

senescence, as measured by increases in nuclear γH2AX (a), p21 mRNA (b) and IL-6 protein (c). Included are representative fluorescence images of γH2AX and cytochemical staining for SA-β-Gal (d). Quantitative data were analyzed by Friedman's ANOVA with differences between two treatment groups assessed by a Wilcoxon matched pairs signed rank test (*$P<0.05$, $n=5$). Scale bar = 50 micron.

Figure 11. cGAS in AEC senescence. We propose in IPF that damaged mtDNA released into the cytosol of AECs by dysfunctional mitochondria, elicits innate immune responses by binding to PRRs. In particular, cGAS activation in the cytosol by self-DNA evokes a 'sterile' inflammatory response that induces secondary senescence.

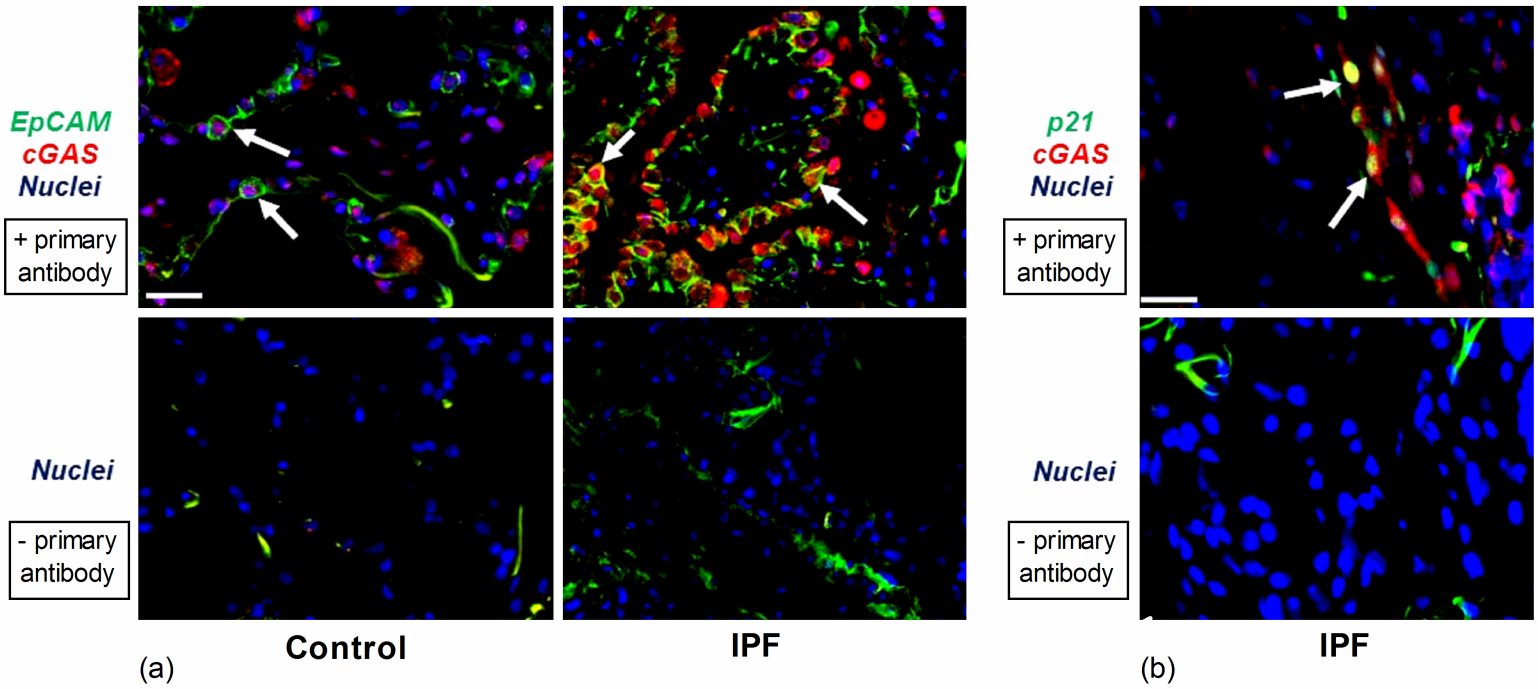

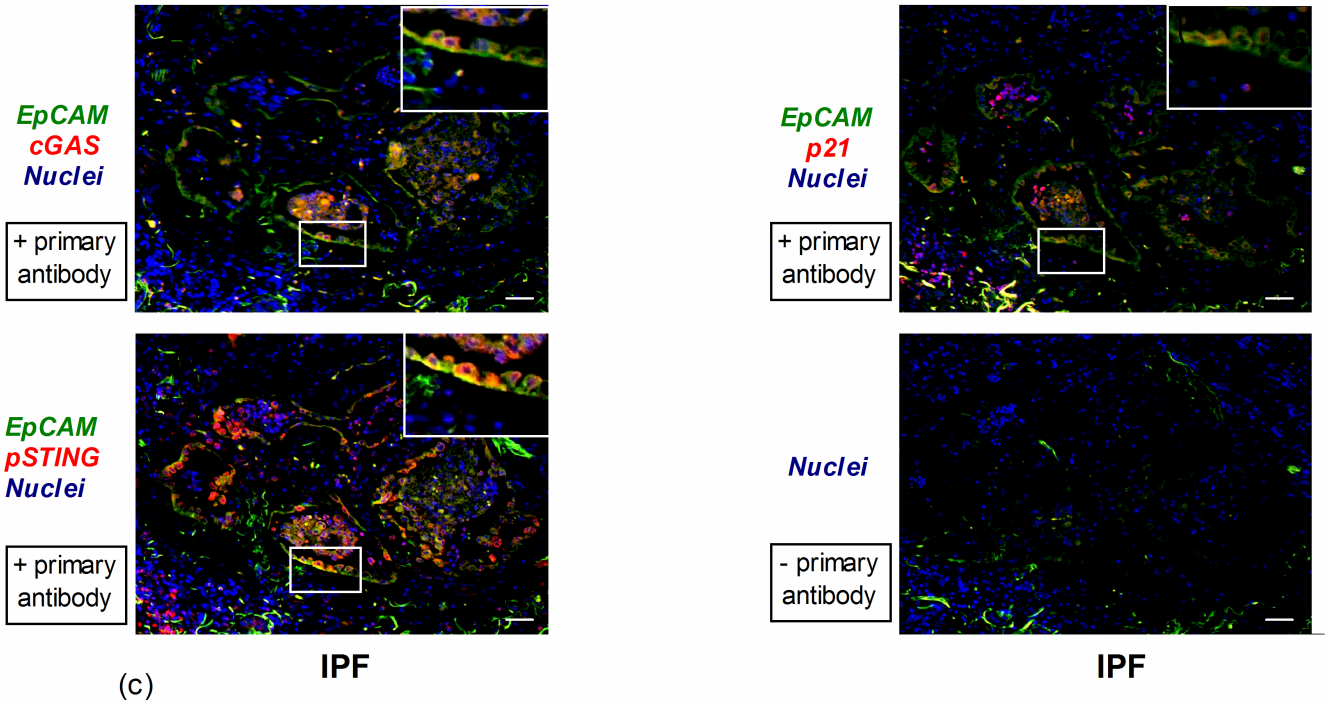

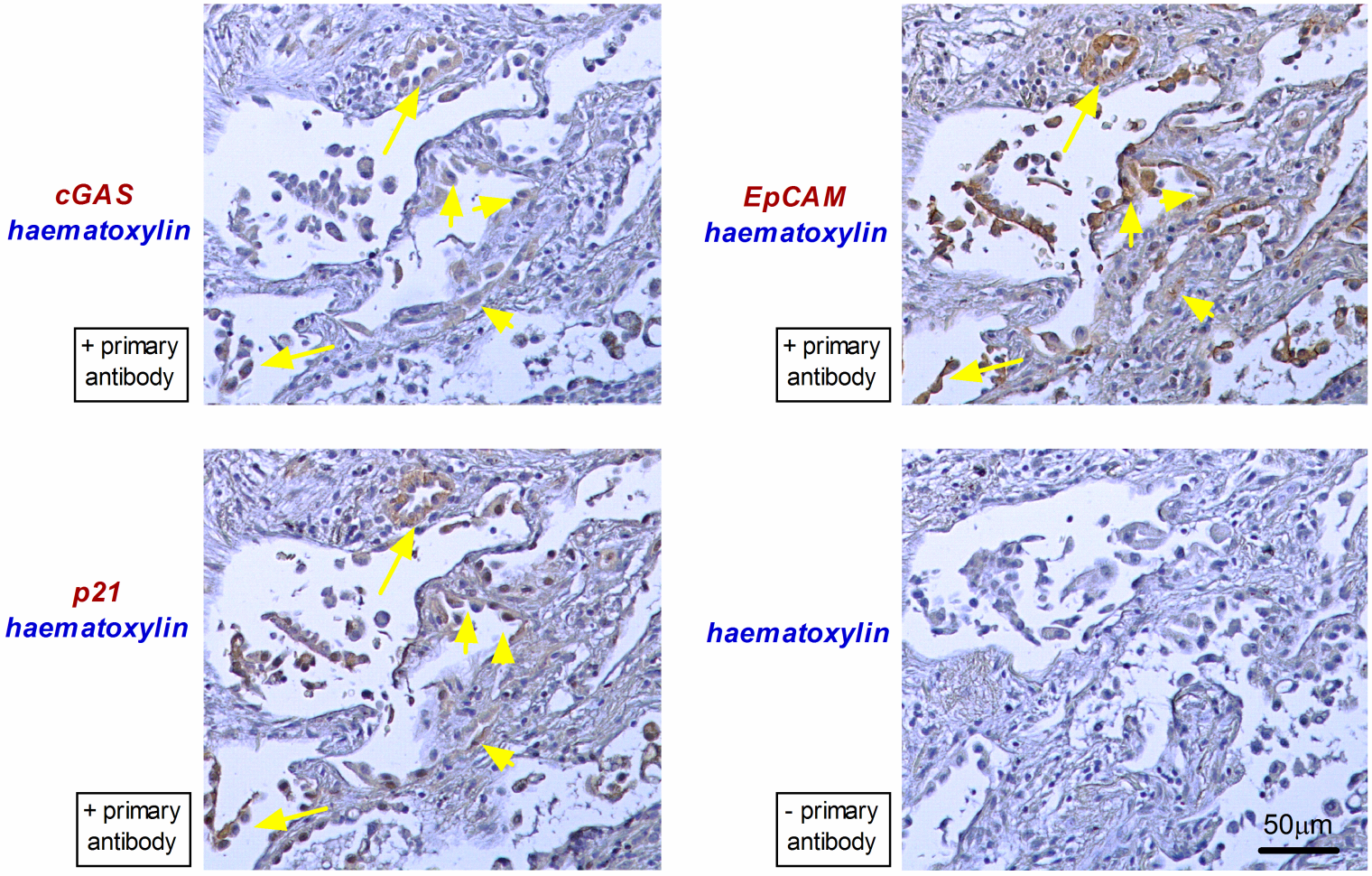

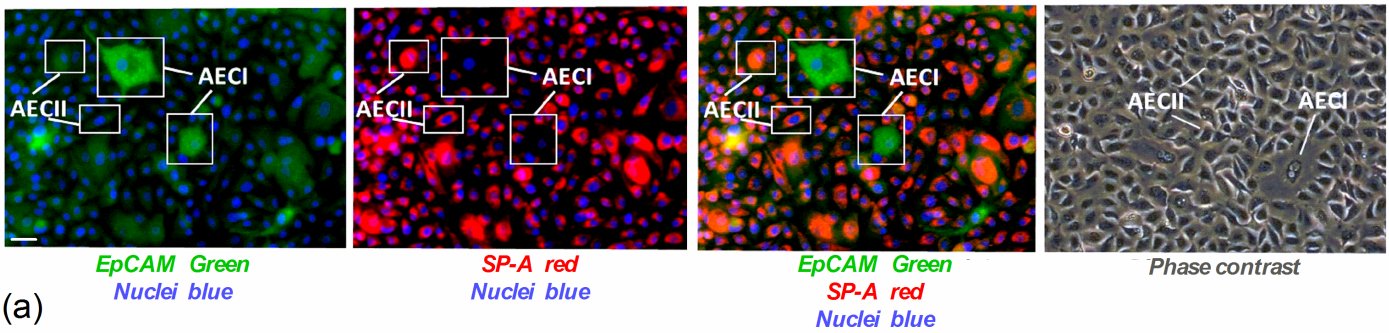

(a)

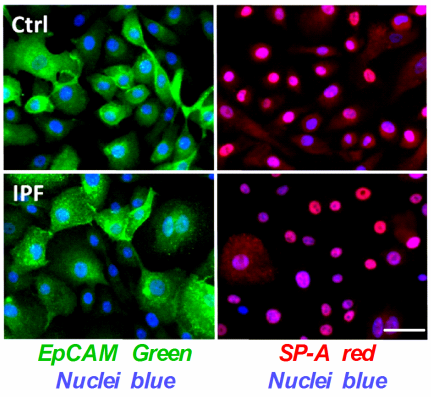

(b)

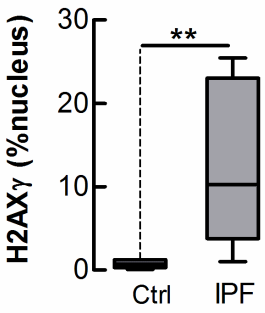

(c)

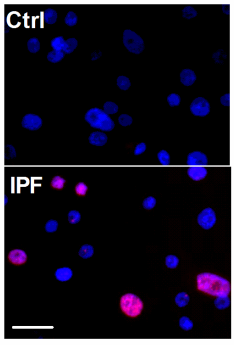

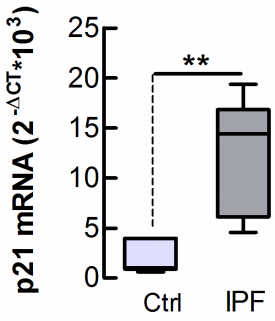

(d)

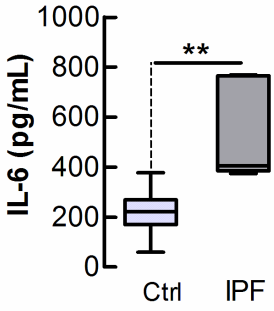

(e)

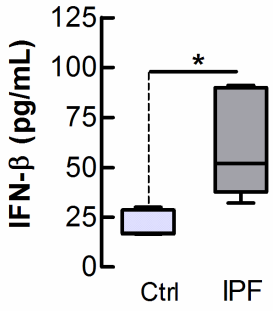

(f)

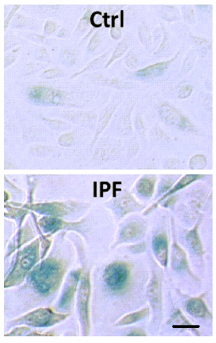

(g)

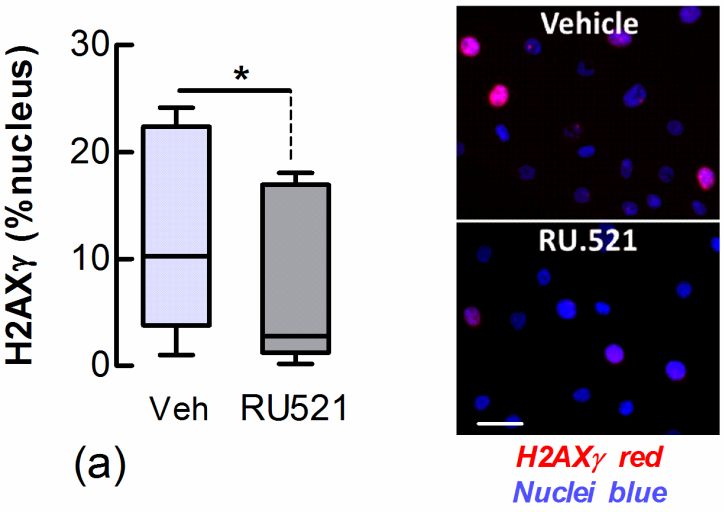

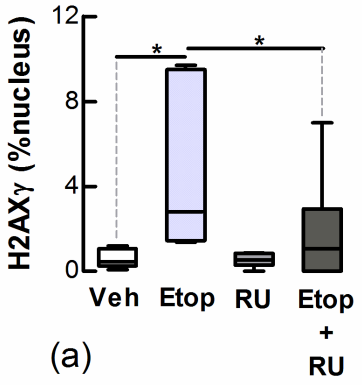

(a)

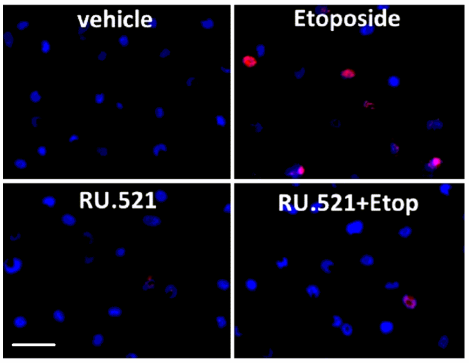

H2AXγ red
Nuclei blue

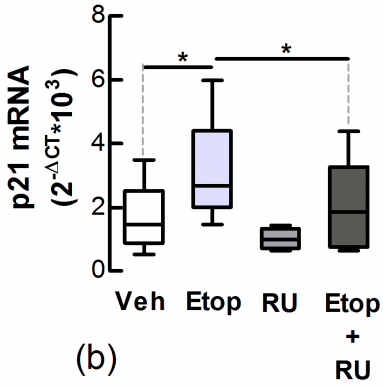

(b)

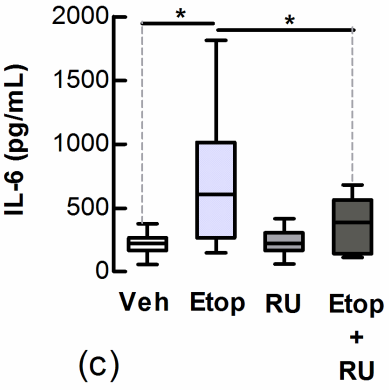

(c)

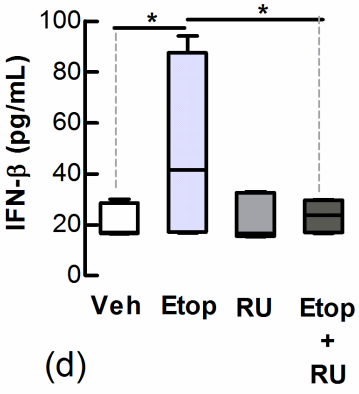

(d)

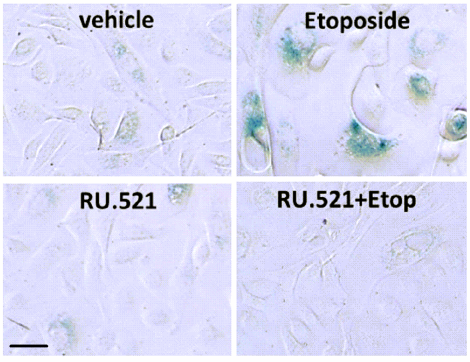

SA-β-Gal blue

(e)

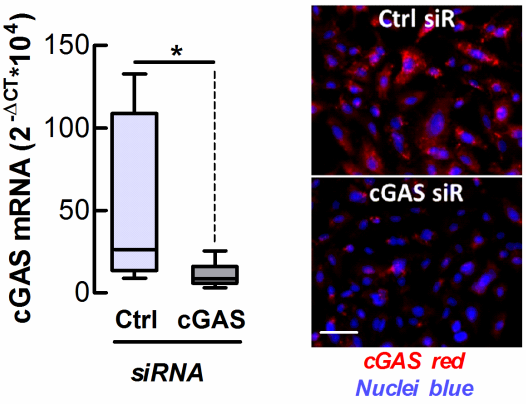

(a)

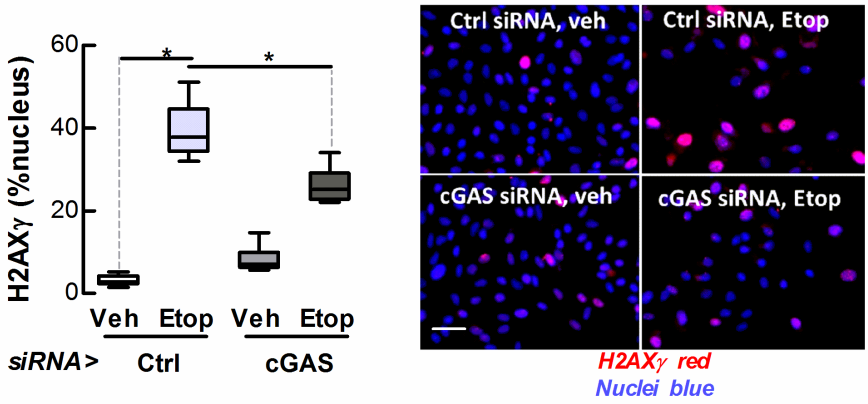

(b)

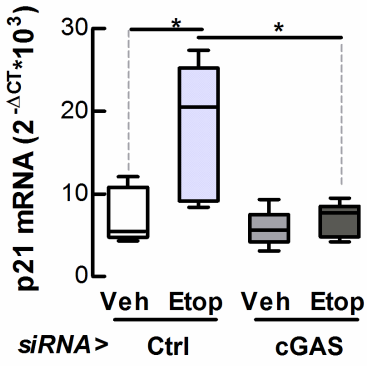

(c)

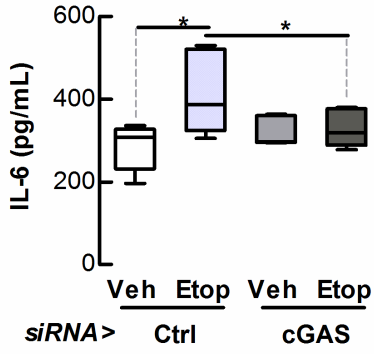

(d)

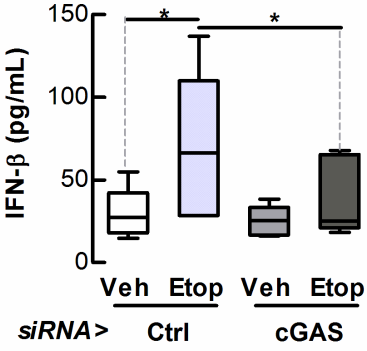

(e)

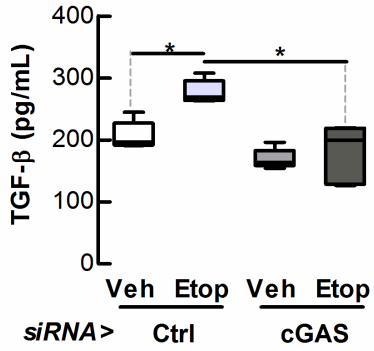

(f)

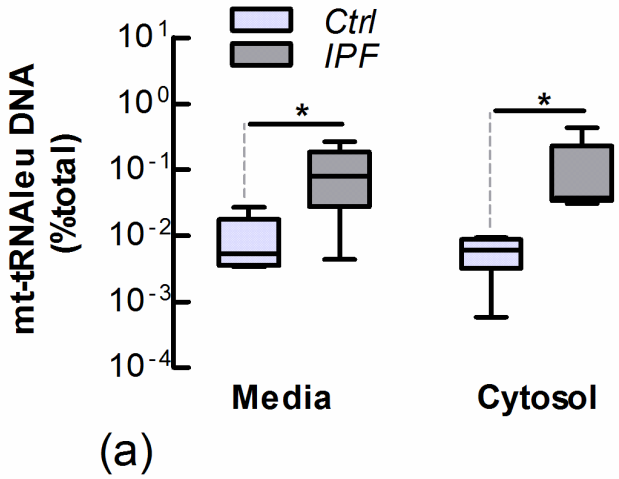

(a)

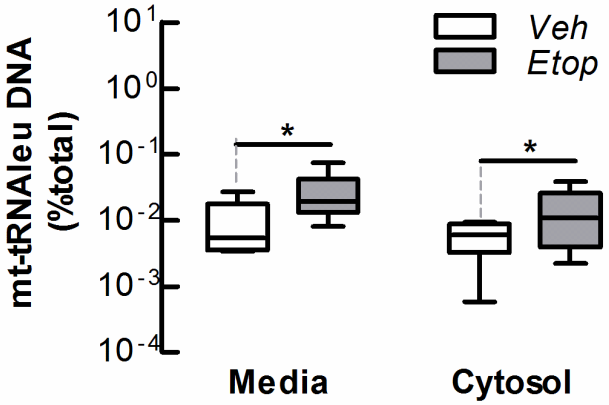

(b)

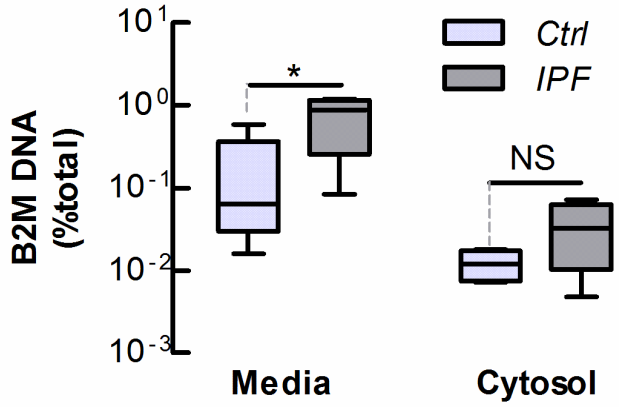

(c)

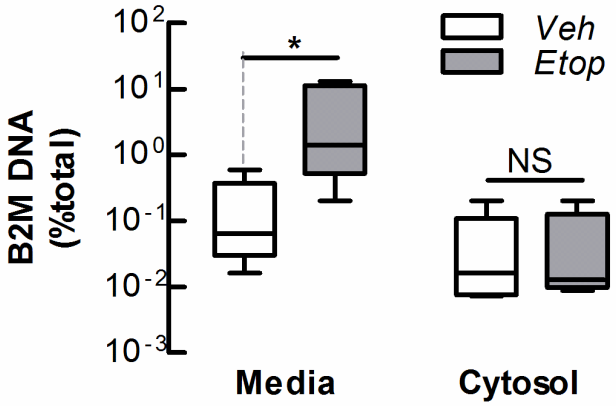

(d)

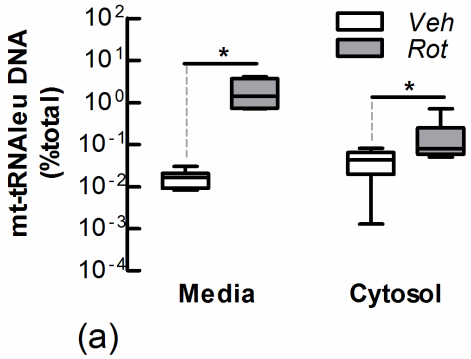

(a)

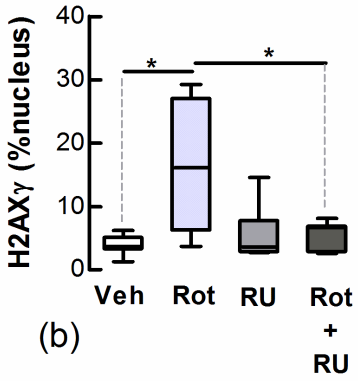

(b)

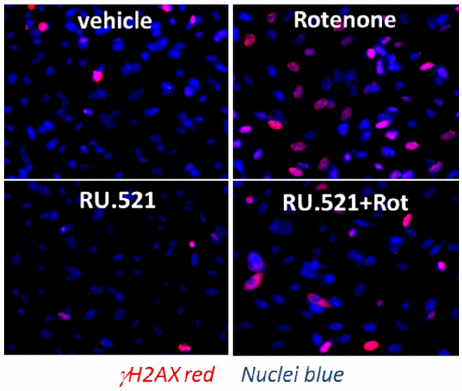

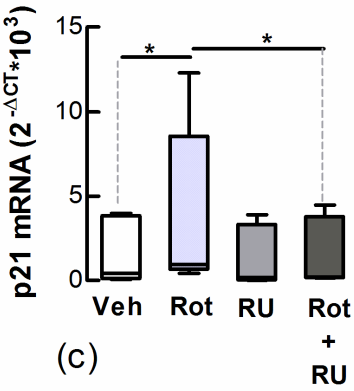

(c)

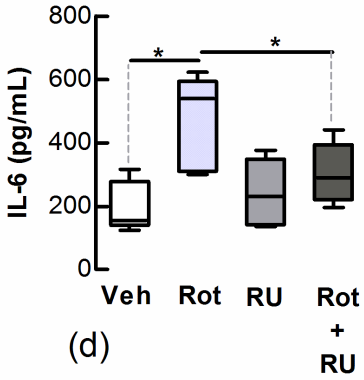

(d)

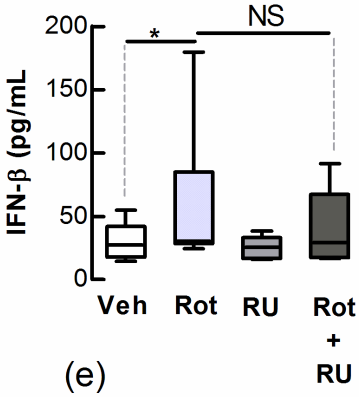

(e)

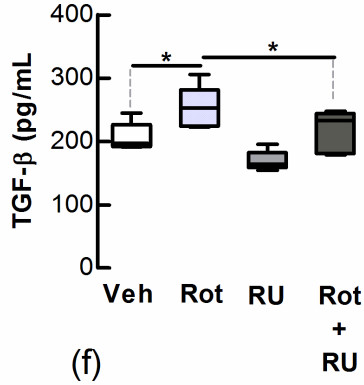

(f)

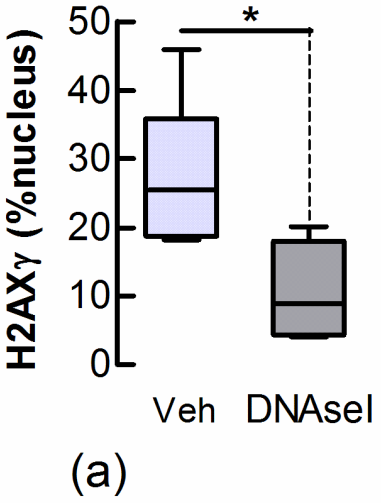

(a)

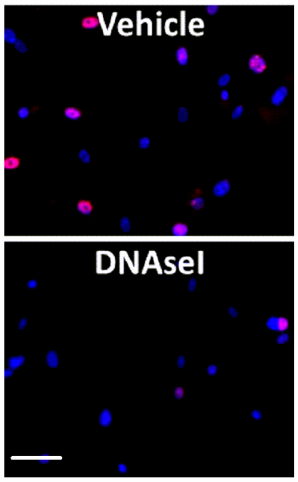

H2AXγ red
Nuclei blue

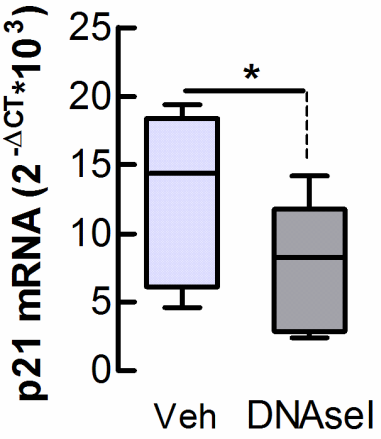

(b)

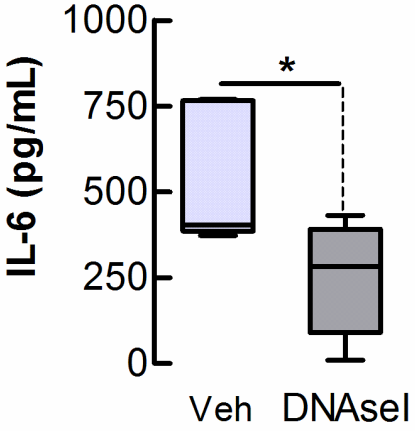

(c)

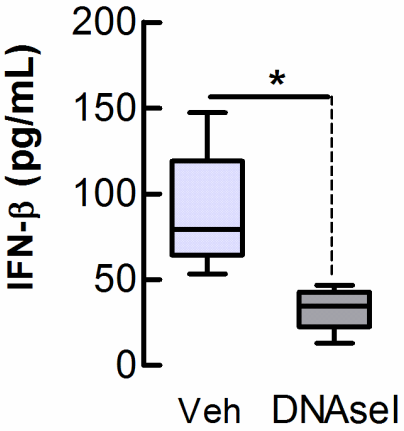

(d)

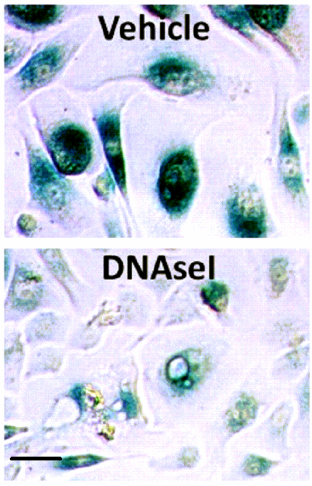

SA-β-Gal blue

(e)

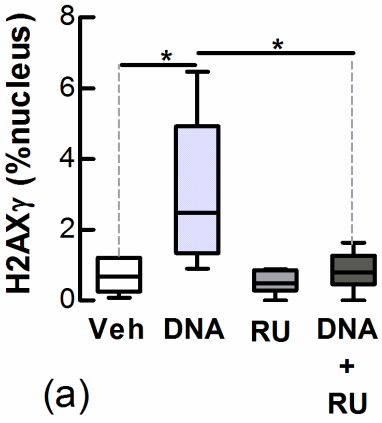

(a)

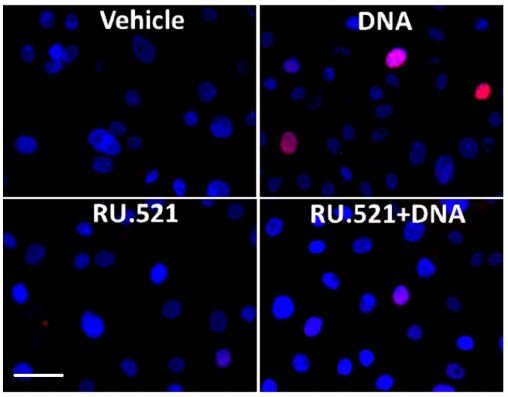

H2AXγ red
Nuclei blue

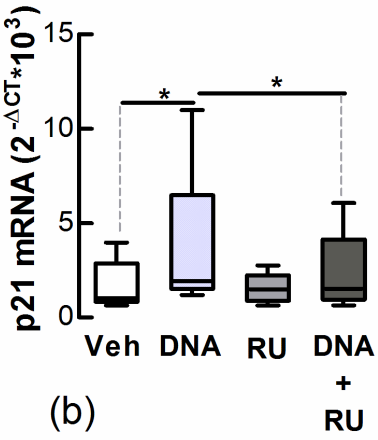

(b)

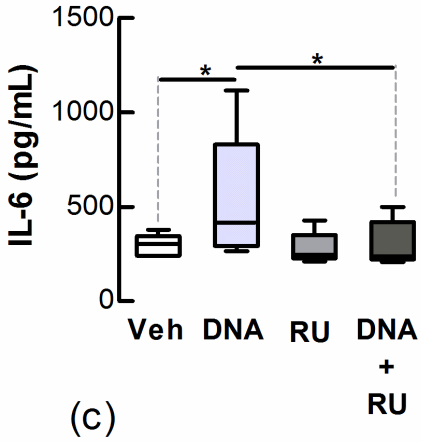

(c)

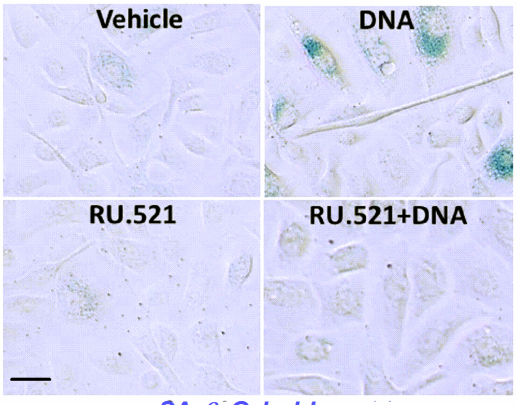

SA-β-Gal blue

(d)